

Self-energy driven resonancelike inelastic neutron spectrum in the s_{++} -wave state in Fe-based superconductors

Lisa Takeuchi, Youichi Yamakawa, and Hiroshi Kontani

Department of Physics, Nagoya University, Furo-cho, Nagoya 464-8602, Japan

 (Received 28 May 2018; revised manuscript received 25 September 2018; published 29 October 2018)

To elucidate the pairing states in Fe-based superconductors, we perform a careful calculation of the dynamical spin susceptibility $\chi^S(\mathbf{q}, \omega)$ at very low temperatures ($T \gtrsim 1$ meV). The feedback effect on both the self-energy and $\chi^S(\mathbf{q}, \omega)$ from the superconducting gap is self-consistently analyzed based on the fluctuation-exchange (FLEX) approximation. In the s_{\pm} -wave state, which has sign reversal in the gap function, $\chi^S(\mathbf{q}, \omega)$ at the nesting momentum $\mathbf{q} = \mathbf{Q}$ shows a resonance peak even when the system is away from the magnetic quantum critical point (QCP). In the s_{++} -wave state that has no sign reversal, $\chi^S(\mathbf{q}, \omega)$ shows a large hump structure when the system is close to the magnetic QCP. This result confirms the validity of a self-energy driven resonancelike peak in the s_{++} -wave state proposed in our previous semimicroscopic study: The enhancement in $\chi^S(\mathbf{q}, \omega)$ due to the self-energy effect exceeds the suppression due to the coherence factor effect near the magnetic QCP. We stress that the hump structure in the s_{++} -wave state given by the FLEX method smoothly changes to a resonancelike sharp peak structure as the system approaches the magnetic QCP, which was not reported in our previous studies. The obtained ω and T dependence of $\chi^S(\mathbf{q}, \omega)$ in the s_{++} -wave states resembles the resonancelike feature in inelastic neutron scattering spectra recently observed in Na(Fe,Co)As and FeSe.

DOI: [10.1103/PhysRevB.98.165143](https://doi.org/10.1103/PhysRevB.98.165143)

I. INTRODUCTION

In Fe-based superconductors, the pairing mechanism and the gap structure with s -wave symmetry have been central open problems. When interpocket repulsive interaction due to the spin fluctuations is strong, the fully gapped sign-reversing s -wave state (the s_{\pm} -wave state) is expected to appear [1,2]. On the other hand, when orbital-fluctuation-driven interpocket attractive interaction is strong, the fully gapped s -wave state without sign reversal (the s_{++} -wave state) will emerge [3–5]. In many optimally doped Fe-based superconductors, nematic orbital fluctuations and spin fluctuations develop cooperatively, as reported in Refs. [6,7]. Theoretically, strong orbital fluctuations are driven by moderate spin fluctuations, thanks to the orbital-spin mode coupling due to the higher-order many-body effects, especially the Aslamazov-Larkin-type vertex correction [8–12].

To detect the presence or absence of the sign reversal in the gap, phase-sensitive experiments are very significant. The nonmagnetic impurity effect provides us with useful phase-sensitive information. In typical d -wave superconductors, like cuprate superconductors and CeCoIn₅, T_c is quickly suppressed by impurities, following the prediction of the Abrikosov-Gor'kov theory [13]. In many Fe-based superconductors, the superconductivity survives even when the residual resistivity due to the randomness is very high, comparable to high- T_c s -wave superconductors MgB₂ and YNi₂B₂C [13,14]. Since the s_{\pm} -wave state is as fragile as the d -wave state theoretically [15,16], these experiments support the (impurity-induced) s_{++} -wave state in optimally doped pnictides [3,17,18].

Another promising phase-sensitive experiment is the inelastic neutron scattering study. A large resonance peak in

the dynamical spin susceptibility appears in d -wave superconductors, such as cuprates [19–21] and CeCoIn₅ [22], reflecting the sign reversal of the d -wave gap [23–26]. In the s_{\pm} -wave state, $\chi^S(\mathbf{q}, \omega)$ is expected to show the resonance peak at $\omega = \omega_{\text{res}} < 2\Delta$ since the coherence factor enlarges the spin fluctuation for the s_{\pm} -wave state [27–32], while it suppresses the spin fluctuation for the s_{++} -wave state. (Δ is the amplitude of the gap function.) Experimentally, clear broad peak structures in $\chi^S(\mathbf{q}, \omega)$ were observed for $T \ll T_c$ in FeSe [33], BaFe_{2-x}Co_xAs₂ [34,35], Ca-Fe-Pt-As [36], Na(Fe,Co)As [37], and (Ba, K)Fe₂As₂ [38]. However, $\chi^S(\mathbf{q}, \omega)$ is drastically modified by not only the coherence factor but also the self-energy effect. In fact, experimentally observed hump structures can be explained based on the s_{++} -wave state [39,40] if one considers the energy dependence of the normal self-energy $\Sigma(\mathbf{k}, \omega)$. This effect is totally dropped in the random-phase-approximation (RPA). Previous theoretical studies [39,40] claim that the peak energy ω_{res} of the hump structure in the s_{++} -wave state satisfies the relation $\omega_{\text{res}} \gtrsim 2\Delta$.

To distinguish between the resonance peak and the hump structure experimentally, it is important to verify the resonance condition $\omega_{\text{res}} < 2\Delta$. However, it is very difficult to obtain the accurate gap amplitude Δ experimentally. In addition, from the theoretical viewpoint, we cannot rule out the relation $\omega_{\text{res}} < 2\Delta$ in the s_{++} -wave state if the system is very close to the magnetic quantum critical point (QCP), as we will discuss in this paper.

The main player in realizing the hump structure of the s_{++} -wave state is the ω dependence of the inelastic quasiparticle damping $\gamma_k^*(\omega) \equiv -\text{Im}\Sigma^R(\mathbf{k}, \omega)/Z(\mathbf{k}, \omega)$, where $Z(\mathbf{k}, \omega)$ is the mass-enhancement factor. Above T_c , $\chi^S(\mathbf{q}, \omega)$ is strongly suppressed by large $\gamma_k^*(\omega)$. Since $\gamma_k^*(\omega) \approx 0$ for $\omega < 3\Delta$ for

$T \ll T_c$, $\chi^S(\mathbf{q}, \omega)$ takes large hump structures at $\omega \gtrsim 2\Delta$. Despite the significance of $\gamma_k^*(\omega)$, the authors of Refs. [39,40] assumed a very simple functional form of $\gamma_k^*(\omega)$, just as a phenomenological function. In addition, the renormalization effect due to the real part of $\Sigma(\mathbf{k}, \omega)$ was dropped. In order to verify the hump-structure mechanism in the s_{++} -wave state without ambiguity, the self-consistent calculation between $\chi^S(\mathbf{q}, \omega)$ and $\Sigma(\mathbf{k}, \omega)$ should be performed at sufficiently low temperatures.

In this paper, we study the dynamical spin susceptibility $\chi^S(\mathbf{q}, \omega)$ in order to elucidate the pairing states in Fe-based superconductors. We self-consistently calculate $\chi^S(\mathbf{q}, \omega)$ and the normal self-energy $\Sigma(\mathbf{k}, \omega)$ using the fluctuation-exchange (FLEX) approximation [23,26,41–50]. We develop the multistep FLEX procedure to perform precise numerical studies at very low temperatures ($T \gtrsim 1$ meV) and analyze the feedback effect on $\Sigma(\mathbf{k}, \omega)$ and $\chi^S(\mathbf{q}, \omega)$ from the superconducting gap carefully. In the s_{\pm} -wave state, $\chi^S(\mathbf{q}, \omega)$ shows the resonance peak even when the system is away from the magnetic QCP. In the s_{++} -wave state, $\chi^S(\mathbf{q}, \omega)$ shows large hump structures near the magnetic QCP since the enhancement in $\chi^S(\mathbf{q}, \omega)$ due to the self-energy effect exceeds the suppression due to the coherence factor effect. This result confirms the validity of the self-energy driven resonancelike peak in the s_{++} -wave state, which was proposed in our previous semimicroscopic study [39,40]. We stress that the hump structure in the s_{++} -wave state smoothly changes to a resonancelike sharp peak as the system approaches the magnetic QCP, which was not reported previously [39,40]. The obtained ω and T dependence of $\chi^S(\mathbf{q}, \omega)$ in the s_{++} -wave states near the magnetic QCP resembles the inelastic neutron scattering spectra in Na(Fe,Co)As [37] and FeSe [33].

Mathematically, the resonance peak appears in the case in which the dynamical spin Stoner factor $\alpha_S(\omega)$ reaches unity for $\omega < 2\Delta$. We show that $\alpha_S(\omega_{\text{res}}) \approx 1$ is realized even in the s_{++} -wave state near the magnetic QCP if the (ω, T) dependence of the self-energy is taken into account correctly.

II. MODEL

A. Hubbard model

The Hamiltonian used is the two-dimensional five-orbital Hubbard model [15]

$$H = \sum_{ij} \sum_{lm} \sum_{\sigma} t_{ij}^{lm} c_{i l \sigma}^{\dagger} c_{j m \sigma} + H_{\text{Coulomb}}, \quad (1)$$

where i, j are the Fe sites, l, m represent the d orbitals, and σ is the spin index. The interaction potentials included are the intraorbital Coulomb potential U , interorbital Coulomb potential U' , Hund's coupling J , and pair hopping J' . The hopping parameters used are those of 1111-type iron-based superconductors, and the Fermi surface obtained is shown in Fig. 1.

Using this Hamiltonian, we solve the 10×10 Nambu Green's function for the superconducting state in the orbital representation,

$$\widehat{G}(k) = \begin{pmatrix} \widehat{G}(k) & \widehat{F}(k) \\ \widehat{F}^{\dagger}(k) & -\widehat{G}^{\dagger}(-k) \end{pmatrix}, \quad (2)$$

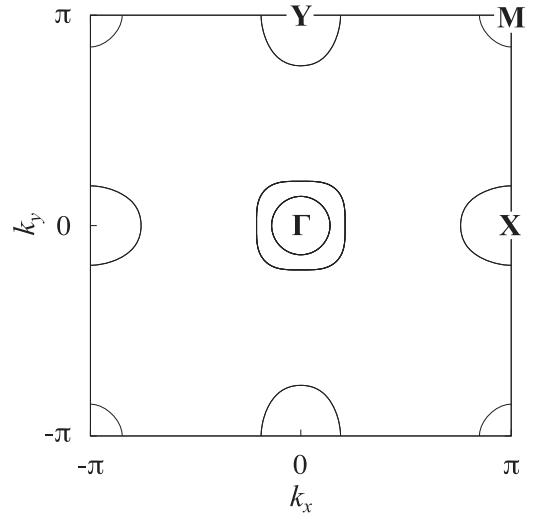


FIG. 1. Fermi surface of 1111-type iron-based superconductors.

where $k = (\mathbf{k}, i\epsilon_n)$. This can be calculated from finding the inverse of the following matrix:

$$\widehat{G}^{-1}(k) = i\epsilon_n \widehat{1} - \begin{pmatrix} \widehat{H}(k) + \widehat{\Sigma}(k) & \widehat{\Delta}(k) \\ \widehat{\Delta}^{\dagger}(k) & -\widehat{H}^{\dagger}(-k) - \widehat{\Sigma}^{\dagger}(-k) \end{pmatrix}, \quad (3)$$

where $\widehat{1}$ is the identity matrix, $\widehat{\Delta}$ is the superconducting gap without renormalization, and $\epsilon_n = \pi T(2n + 1)$ is the Matsubara frequency for fermions. $\widehat{\Sigma}$ is the normal self-energy, which represents the mass enhancement and quasiparticle damping. In this study, we introduce $\widehat{\Delta}$ as a parameter.

B. Gap functions

To calculate the spin susceptibility in superconducting state, we introduce the “unrenormalized gap functions” in Eq. (3). In each band, we introduce the following s_{++} - and s_{\pm} -wave gap functions in the band representation:

$$s_{++} : \Delta(\mathbf{k}) = \Delta_0, \quad (4)$$

$$s_{\pm} : \Delta(\mathbf{k}) = \Delta_0[\cos(k_x) + \cos(k_y)]. \quad (5)$$

To calculate the temperature dependence of spin susceptibility, we introduce a superconducting gap with a BCS-like temperature dependence, $\Delta_0(T) = \Delta_0(0) \tanh[1.74\sqrt{(T_c/T) - 1}]$.

Hereafter, in the numerical study using the FLEX approximation, we set $T_c = 8$ meV and $\Delta_0(T = 0) = 50$ meV unless otherwise noted. The physical gap function is given as $\Delta^*(\mathbf{k}) \approx \Delta(\mathbf{k})/Z(\mathbf{k})$, where $Z(\mathbf{k}) = 1 - \frac{\partial}{\partial \omega} \Sigma(\mathbf{k}, \omega)|_{\omega=0}$ is the mass-enhancement factor given by the normal self-energy.

In optimally doped Fe-based superconductors, the energy scale of spin and/or orbital fluctuations, which gives the pairing glue, is small. For this reason, $\Delta(\mathbf{k})$ should be large only near the Fermi level. To express this fact [51], we introduce the following high-energy cutoff for the gap function:

$$\Delta_c(\mathbf{k}) = \Delta(\mathbf{k}) \cdot \frac{\epsilon_{\text{cut}}^2}{[\epsilon(\mathbf{k}) - \mu]^2 + \epsilon_{\text{cut}}^2}, \quad (6)$$

with $\epsilon_{\text{cut}} = 4\Delta_0$. The gap function in the orbital representation can be expressed as

$$[\widehat{\Delta}(\mathbf{k})]_{lm} = \sum_b U_{lb}(\mathbf{k})U_{mb}^\dagger(\mathbf{k})\Delta_e(\mathbf{k}), \quad (7)$$

where $U_{lb}(\mathbf{k})$ is the unitary matrix element and b represents the conduction band number.

C. FLEX approximation

The FLEX approximation is a method to calculate self-energy and susceptibilities in a self-consistent manner. The feedback effect from spin fluctuation is included by using the FLEX approximation, allowing a microscopic calculation of the system.

The bare susceptibilities in the Matsubara frequency representation are written as

$$\chi_{ll'mm'}^0(q) = -\frac{T}{N} \sum_k G_{lm}(k+q)G_{m'l'}(k), \quad (8)$$

$$\phi_{ll'mm'}^0(q) = -\frac{T}{N} \sum_k F_{lm'}(k+q)F_{l'm}^\dagger(k), \quad (9)$$

where $q = (\mathbf{q}, i\omega_l)$, $\omega_l = 2\pi lT$, and N is the number of \mathbf{k} meshes. The spin and charge susceptibilities are

$$\chi_{ll'mm'}^S(q) = \left[\frac{\widehat{\chi}^0(q) + \widehat{\phi}^0(q)}{1 - \widehat{\Gamma}^S[\widehat{\chi}^0(q) + \widehat{\phi}^0(q)]} \right]_{ll'mm'}, \quad (10)$$

$$\chi_{ll'mm'}^C(q) = \left[\frac{\widehat{\chi}^0(q) - \widehat{\phi}^0(q)}{1 - \widehat{\Gamma}^C[\widehat{\chi}^0(q) - \widehat{\phi}^0(q)]} \right]_{ll'mm'}, \quad (11)$$

where $\widehat{\Gamma}^S$ and $\widehat{\Gamma}^C$ are the spin and charge interaction matrices, respectively [9].

The Feynman diagrams considered in the calculation of self-energy are the bubble terms and ladder terms. Normal self-energy in the superconducting state is calculated by the expression

$$\Sigma_{lm}(k) = \frac{T}{N} \sum_q \sum_{l'm'} G_{l'm'}(k-q)V_{ll'mm'}(q). \quad (12)$$

The interaction part $V_{ll'mm'}(q)$ is

$$\begin{aligned} V_{ll'mm'}(q) &= \frac{3}{2}V_{ll'mm'}^S(q) + \frac{1}{2}V_{ll'mm'}^C(q) \\ &- \sum_{l_1 l_2 l_3 l_4} \left[+\frac{1}{4}\Gamma_{ll'l_1 l_2}^{\uparrow\uparrow} \chi_{l_1 l_2 l_3 l_4}^0(q) \Gamma_{l_3 l_4 mm'}^{\uparrow\uparrow} \right. \\ &+ \frac{1}{2}\Gamma_{ll'l_1 l_2}^{\uparrow\downarrow} \chi_{l_1 l_2 l_3 l_4}^0(q) \Gamma_{l_3 l_4 mm'}^{\uparrow\downarrow} \\ &- \frac{1}{2}\Gamma_{ll'l_1 l_2}^{\uparrow\uparrow} \phi_{l_1 l_2 l_3 l_4}^0(q) \Gamma_{l_3 l_4 mm'}^{\uparrow\downarrow} \\ &\left. - \frac{1}{2}\Gamma_{ll'l_1 l_2}^{\uparrow\downarrow} \phi_{l_1 l_2 l_3 l_4}^0(q) \Gamma_{l_3 l_4 mm'}^{\uparrow\uparrow} \right]. \quad (13) \end{aligned}$$

Here, we define $\widehat{V}^{S(C)} = \widehat{\Gamma}^{S(C)}\widehat{\chi}^{S(C)}\widehat{\Gamma}^{S(C)}$, $\widehat{\Gamma}^{\uparrow\uparrow} = (\widehat{\Gamma}^C + \widehat{\Gamma}^S)/2$, and $\widehat{\Gamma}^{\uparrow\downarrow} = (\widehat{\Gamma}^C - \widehat{\Gamma}^S)/2$. For the numerical study of the spin susceptibility, we derive the retarded (advanced) self-energy $\widehat{\Sigma}^{R(A)}(\mathbf{k}, \epsilon)$ from $\widehat{\Sigma}(\mathbf{k}, i\epsilon_n)$ given by the FLEX by performing the numerical analytic continuation.

D. Spin susceptibility

The normal bare susceptibility $\chi^{0,R}$ and the anomalous bare susceptibility $\phi^{0,R}$ in the real-energy representation can be expressed by the following equations [26,40]:

$$\begin{aligned} \chi_{ll'mm'}^{0,R}(\mathbf{q}, \omega) &= \frac{-1}{4\pi i N} \sum_k \\ &\times \left[\int_{-\infty}^{\infty} dz \tanh\left(\frac{z}{2T}\right) G_{lm}^R(\mathbf{k}^+, z^+) \rho_{m'l'}^G(\mathbf{k}, z) \right. \\ &\left. + \int_{-\infty}^{\infty} dz \tanh\left(\frac{z}{2T}\right) \rho_{lm}^G(\mathbf{k}^+, z^+) G_{m'l'}^A(\mathbf{k}, z) \right], \quad (14) \end{aligned}$$

$$\begin{aligned} \phi_{ll'mm'}^{0,R}(\mathbf{q}, \omega) &= \frac{-1}{4\pi i N} \sum_k \\ &\times \left[\int_{-\infty}^{\infty} dz \tanh\left(\frac{z}{2T}\right) F_{lm'}^R(\mathbf{k}^+, z^+) \rho_{m'l'}^{F^\dagger}(\mathbf{k}, z) \right. \\ &\left. + \int_{-\infty}^{\infty} dz \tanh\left(\frac{z}{2T}\right) \rho_{lm'}^F(\mathbf{k}^+, z^+) F_{m'l'}^{\dagger A}(\mathbf{k}, z) \right]. \quad (15) \end{aligned}$$

Here, $\rho_{ll'}^G = (G_{ll'}^A - G_{ll'}^R)/2\pi i$, and $\rho_{ll'}^{F^\dagger} = (F_{ll'}^{\dagger A} - F_{ll'}^{\dagger R})/2\pi i$. G^A , F^A are the advanced Green's functions, and G^R , F^R are the retarded Green's functions. We define $\mathbf{k}^+ = \mathbf{k} + \mathbf{q}$ and $z^+ = z + \omega$ for simplicity.

The spin susceptibility $\chi^{S,R}$ can be expressed by

$$\chi_{ll'mm'}^{S,R}(\mathbf{q}, \omega) = \left[\frac{\widehat{\chi}^{0,R}(\mathbf{q}, \omega) + \widehat{\phi}^{0,R}(\mathbf{q}, \omega)}{1 - \widehat{\Gamma}^S[\widehat{\chi}^{0,R}(\mathbf{q}, \omega) + \widehat{\phi}^{0,R}(\mathbf{q}, \omega)]} \right]_{ll'mm'}. \quad (16)$$

Here, we introduce the Stoner factor α_S defined as the maximum eigenvalue of

$$\widehat{\Gamma}^S[\widehat{\chi}^{0,R}(\mathbf{q}, 0) + \widehat{\phi}^{0,R}(\mathbf{q}, 0)]. \quad (17)$$

It is proportional to the strength of the spin fluctuation; χ^S diverges when α_S is 1.

The results of neutron scattering experiments correspond to the imaginary part of the spin susceptibility,

$$\text{Im}\chi^S(\mathbf{Q}, \omega) = \text{Im} \left[\sum_{lm} \chi_{llmm}^{S,R}(\mathbf{Q}, \omega) \right]. \quad (18)$$

III. RESULTS

In order to calculate at low temperatures, the multistep method is used in this research. We present the explanation for this method in Appendix A. Results for the FLEX approximation and RPA are calculated with a \mathbf{k} mesh of 128^2 and Matsubara frequency of 2^{16} . Bare susceptibilities in the energy representation [Eqs. (14) and (15)] are calculated with a \mathbf{k} mesh of 256^2 and an energy range divided by 2^{12} ($\delta z \sim 1$ meV).

In this section, we perform a self-consistent numerical study based on the FLEX approximation. Except in Fig. 8, we calculate the T dependences of physical quantities for a fixed Coulomb interaction which satisfy the condition $\alpha_S = 0.90-0.97$ at $T = T_c (= 8$ meV).

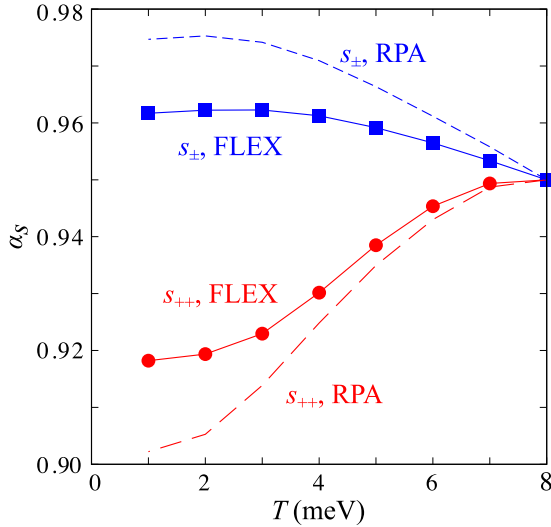


FIG. 2. T dependence of the Stoner factor at the nesting vector \mathbf{Q} given by the RPA ($\Delta_0 = 10$ meV) and by the FLEX ($\Delta_0 = 50$ meV). In each case, $\alpha_S = 0.95$ at T_c . We set $U_{\text{FLEX}} = 2.11$ eV and $U_{\text{RPA}} = 1.13$ eV. Note that $\Delta^* \approx 13$ (9.6) meV for s_{++} (s_{\pm})-wave state, as shown in Fig. 3.

A. Feedback effect

Figure 2 shows the T dependence of the Stoner factor α_S in the superconducting state. The Stoner factor behaves differently for the s_{++} and s_{\pm} states in both the RPA and FLEX approximation. One of the reasons is that $\phi^0(\mathbf{q})$ in the irreducible susceptibility is proportional to $-\Delta(\mathbf{k})\Delta(\mathbf{k} + \mathbf{q})$, which is negative (positive) for s_{++} -wave (s_{\pm} -wave) states at nesting vector $\mathbf{Q} = (\pi, 0)$. By reflecting the difference in sign of this factor, which corresponds to the difference in the coherence factor in the BCS theory, α_S in the s_{++} -wave state is smaller than α_S in the s_{\pm} -wave state. To summarize, α_S slightly decreases in the s_{++} -wave state, whereas it increases in the s_{\pm} -wave state.

The T dependence of α_S obtained by the RPA for $\Delta_0 = 10$ meV is similar to that obtained by the FLEX for $\Delta_0 = 50$ meV for both s_{++} and s_{\pm} states. This result is reasonable because the renormalized gap in the FLEX averaged over the Fermi surfaces is $\Delta^* \approx 13$ (9.6) meV for the s_{++} - (s_{\pm} -) wave state at $T = 1$ meV, as we will discuss in the next subsection.

Figure 3 shows α_S in the superconducting state obtained by the FLEX approximation for $\Delta_0 = 50$ meV in the case of $\alpha_S(T_c) = 0.90$ – 0.97 . In Fig. 3(a) for the s_{++} -wave state, the Stoner factor monotonically decreases with decreasing T in the case of $\alpha_S(T_c) \leq 0.95$. In contrast, the Stoner factor first increases slightly and then decreases at low temperatures in the case of $\alpha_S(T_c) \geq 0.96$. In Fig. 3(b) for the s_{\pm} -wave state, the Stoner factor is almost constant when $\alpha_S(T_c) \leq 0.90$. In contrast, the Stoner factor monotonically increases with decreasing T when $\alpha_S(T_c) \geq 0.95$.

Thus, when the system is close to the magnetic QCP in the normal state, the spin fluctuations remain strong even in the s_{++} -wave superconducting states. The reason is the following: in the normal state at $T \geq T_c$, $\chi^S(\mathbf{q}, \omega = 0)$ is suppressed by the large inelastic scattering $\gamma_k(\omega)$ for $\omega \sim 0$. [Here, $\gamma_k(\omega)$ is the imaginary part of the self-energy.] For $T \ll T_c$, $\gamma_k(\omega)$

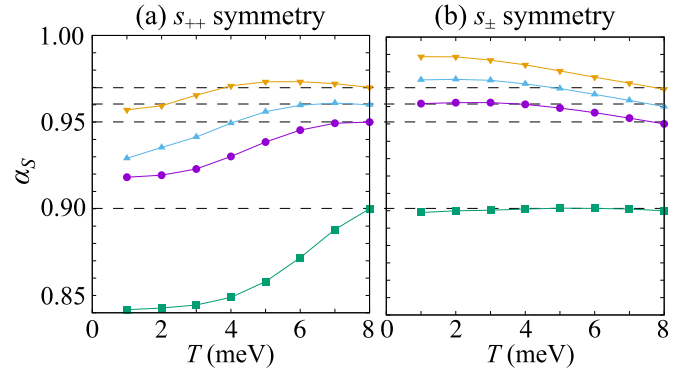


FIG. 3. T dependence of α_S for the initial values $\alpha_S = 0.90$ – 0.97 at $T = T_c$ in the case of (a) the s_{++} -wave state and (b) the s_{\pm} -wave state.

is prominently reduced for $|\omega| < 3\Delta^*$ (see Sec. III C), which leads to the increment of $\chi^S(\mathbf{q}, \omega = 0)$. Therefore, the self-energy gives the positive feedback from the superconducting gap to the spin susceptibility for both the s_{++} and s_{\pm} states. To summarize, both the coherence factor and the self-energy effect are important for understanding the spin fluctuations in the superconducting state.

B. Renormalized gap size Δ^*

By including the normal self-energy, the original gap Δ_0 in Eq. (5) is renormalized to be the physical gap function Δ^* . Figure 4 shows both Δ_0 and Δ^* obtained by the FLEX approximation; $\alpha_S(T_c) = 0.95$. The size of Δ^* is estimated numerically from the relation $1/\text{Re}F(\mathbf{k}, \omega) = 0$ on the Fermi surfaces. In the s_{++} -wave state, $2\Delta^* \approx 13$ meV, so the relation $2\Delta^*/T_c \approx 3.3$ holds at $T = 1$ meV. The ratio $2\Delta^*/T_c$ increases to 4.3 if we set $T_c = 6$ meV. We remark that the numerical result of $\chi^S(\mathbf{q}, \omega)$ is insensitive to T_c in the case $T \lesssim 0.5T_c$.

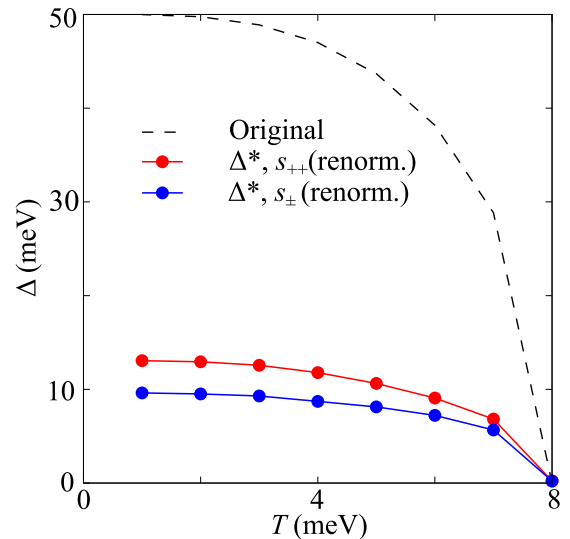


FIG. 4. Renormalized superconducting gap Δ^* given by the FLEX approximation, for both the s_{++} - and s_{\pm} -wave states. The original unphysical gap Δ_0 is also plotted.

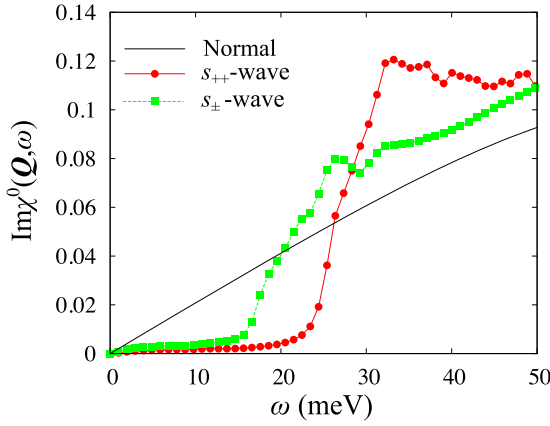


FIG. 5. The ω dependence of $\text{Im}\chi^0(\mathbf{Q}, \omega)$ at $T = 3$ meV for both the s_{++} and s_{\pm} states. In each state, we set $\alpha_S(T_c) = 0.95$. The result for the normal state ($T = T_c = 8$ meV) is plotted for comparison. $\Delta^* \approx 13$ meV (9.6 meV) for the s_{++} wave (s_{\pm} wave).

We can also derive Δ^* from the energy dependence of $\text{Im}\chi^0(\mathbf{Q}, \omega)$. Since $\text{Im}\chi^0(\mathbf{Q}, \omega)$ is the absorption spectrum of particle-hole scattering, it should be zero for $|\omega| < 2\Delta^*$ at zero temperatures. Figure 5 shows the $\text{Im}\chi^0(\mathbf{Q}, \omega)$ obtained by the FLEX at $T = 3$ meV for both the s_{++} - and s_{\pm} -wave states. From the result, Δ^* is estimated to be 10–15 meV for both the s_{++} -wave and s_{\pm} -wave states, consistent with the results in Fig. 4.

C. Damping γ due to inelastic scattering

Figure 6 shows the energy dependence of quasiparticle damping, $\gamma(\mathbf{k}, \omega) = -\sum_l \text{Im}[\Sigma_{ll}^R(\mathbf{k}, \omega)]$, given by the FLEX approximation. Compared to the normal state ($T = T_c$), the damping in the superconducting state ($T = 3$ meV) is drastically suppressed for the lower-energy region. In the s_{++} -wave

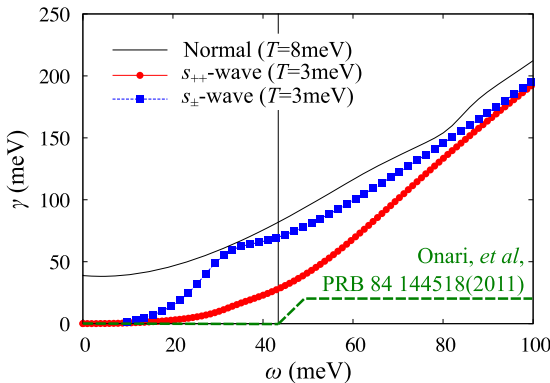


FIG. 6. Energy dependence of $\gamma(\mathbf{k}, \omega)$ at $\mathbf{k} = (0.74\pi, 0)$ given by the FLEX approximation. We set $\alpha_S = 0.95$ in the normal state at $T = T_c = 8$ meV. In this case, Fermi liquid behavior $\gamma(\omega) \approx \gamma_0 + a\omega^2$ is obtained. The low-energy ($\omega \sim 0$) inelastic scattering is strongly suppressed in both the s_{++} - and s_{\pm} -wave states. The oversimplified phenomenological damping rate introduced in previous research [40] is plotted for comparison. Note that the renormalized quasiparticle damping is $\gamma^* = \gamma/Z$, where Z is the mass-enhancement factor ($Z \sim 5$).

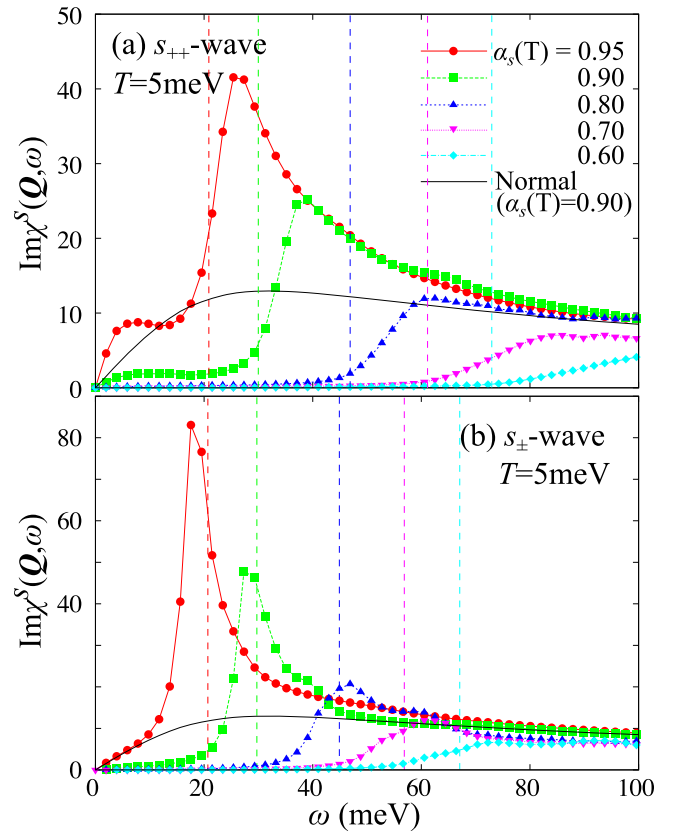


FIG. 7. Energy dependence of $\text{Im}\chi^S$ for (a) s_{++} - and (b) s_{\pm} -wave states for $\alpha_S(T) = 0.95$ –0.6 at $T = 5$ meV. Each calculation is in the superconducting state with $\Delta_0 = 50$ meV. The values of Δ^* for each $\alpha_S(T)$ are shown by vertical dashed lines.

state, $\gamma(\mathbf{k}, \omega)$ is suppressed for $|\omega| < 3\Delta^*$ [40]. The reason is as follows: in the inelastic scattering process, the initial quasiparticle with energy E_i should create a particle-hole excitation with $E_{ph} > 2\Delta^*$, and the final quasiparticle should satisfy $E_f > \Delta^*$. Thus, the relation $E_i = E_{ph} + E_f > 3\Delta^*$ is required at $T = 0$. In the s_{\pm} -wave state, $\gamma(\mathbf{k}, \omega)$ is large even for $|\omega| \lesssim 3\Delta^*$ since the low-energy collective resonance mode ($\omega_{\text{res}} < 2\Delta^*$; see Sec. III D) contributes to the low-energy inelastic scattering processes.

D. Calculations for the neutron scattering experiment

Here, we explain the dynamical susceptibility $\chi^S(\mathbf{q}, \omega)$ obtained by the FLEX approximation for various parameters in the cases of the s_{++} -wave and s_{\pm} -wave states. The resonance-like hump structure in the ω dependence of $\chi^S(\mathbf{q}, \omega)$ appears even in the s_{++} -wave state. This result is consistent with previous RPA analysis in Refs. [39,40].

1. α_S dependence of $\text{Im}\chi^S(\mathbf{q}, \omega)$

Figure 7 shows the ω dependence of $\text{Im}\chi^S(\mathbf{Q}, \omega)$ for various Stoner factors in both the s_{++} -wave [Fig. 7(a)] and s_{\pm} -wave [Fig. 7(b)] states. Calculations are done with parameters $T = 5$ meV and $\Delta_0 = 50$ meV. The nesting vector is $\mathbf{Q} = (\pi, 0)$. In Fig. 7(a) we find that a hump structure is obtained in the s_{++} -wave state, even for moderate spin fluctuations

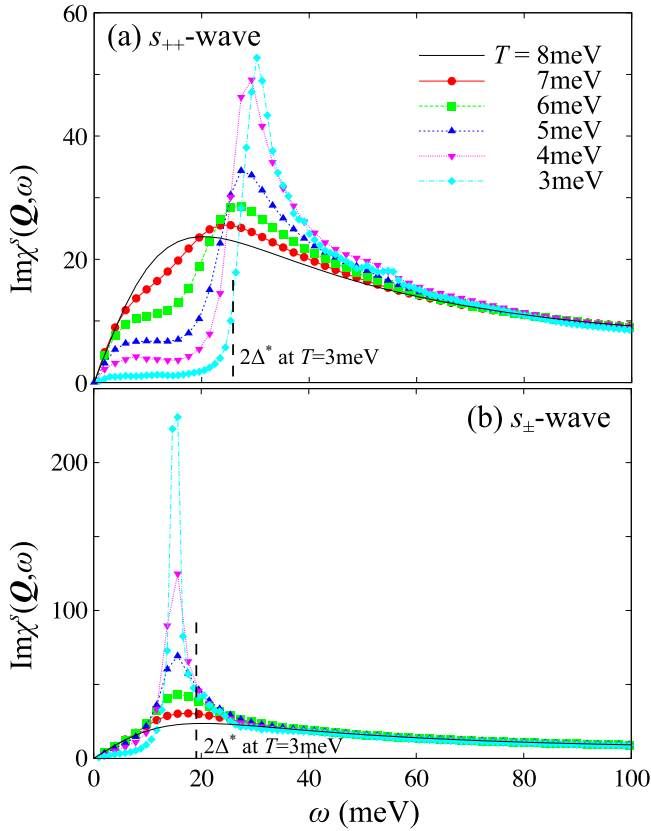


FIG. 8. Energy dependence of $\text{Im}\chi^S$ for (a) s_{++} and (b) s_{\pm} states below T_c . The black line ($T_c = 8$ meV) is the normal state. In the s_{++} -wave state, the height of the peak saturates at low temperatures.

($\alpha_S = 0.90$). The obtained hump structure is similar to the report of previous RPA analysis [40]. As the spin fluctuations become stronger ($\alpha_S = 0.95$), the hump structures become narrower, such that it looks like a resonance peak. The relation $\omega_{\text{res}} \approx 2\Delta^*$ is satisfied. In Fig. 7(b), we see that unlike the s_{++} state, results for the s_{\pm} state have a peaklike structure at small spin fluctuation. The condition of the resonance $\omega_{\text{res}} < 2\Delta^*$ is apparently satisfied for $\alpha_S \geq 0.9$. As α_S is increased, the resonance peak becomes narrower, and ω_{res} decreases.

2. Temperature dependence of $\text{Im}\chi^S(q, \omega)$

Figure 8 shows the ω dependence of $\text{Im}\chi^S(\mathbf{Q}, \omega)$ in the superconducting state $T \leq T_c$ obtained by the FLEX approximation. The lowest temperature is $T = 3$ meV, which is considerably lower than $T_c = 8$ meV. We set $\alpha_S(T_c) = 0.95$. In the case of the s_{++} state shown in Fig. 8(a), the hump structure at $\omega_{\text{res}} \lesssim 30$ meV becomes taller and sharper as T is lowered. The hump structure looks like a resonance peak at the lowest temperature $T = 3$ meV. The energy position ω_{res} slightly increases as T decreases, and ω_{res} is slightly above $2\Delta^*$. Figure 8(b) shows the result for the s_{\pm} state. Compared to the s_{++} state, the magnitude of the structures is much larger, and the resonance energy ω_{res} does not move.

Compared to the result at $T = T_c$, the height of $\text{Im}\chi^S(\mathbf{Q}, \omega)$ in the s_{++} state is approximately two times larger in size, while the height of the resonance peak in the s_{\pm} state is approximately nine times larger. In many Fe-based

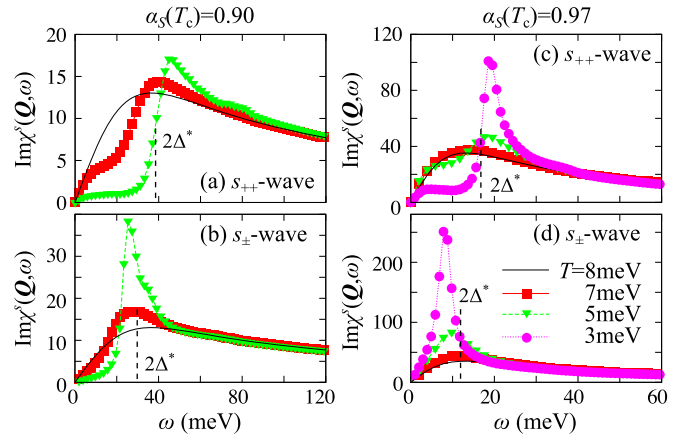


FIG. 9. Energy dependence of $\text{Im}\chi^S$ with $\alpha_S(T_c) = 0.90$ for $T_c \geq T \geq 5$ meV for the (a) s_{++} and (b) s_{\pm} states. Energy dependence of $\text{Im}\chi^S$ with $\alpha_S(T_c) = 0.97$ for $T_c \geq T \geq 3$ meV for the (c) s_{++} and (d) s_{\pm} states. In (c), the relation $\omega_{\text{res}} \approx 2\Delta^*$ holds even in the s_{++} -wave state.

superconductors, the observed “resonance peak” is not so sharp, its weight is not so large, and the height tends to saturate at low temperatures [34,37]. Thus, the obtained $\text{Im}\chi^S(\mathbf{Q}, \omega)$ in the s_{++} state well explains experimental results.

We also examine the spin susceptibility $\text{Im}\chi^S(\mathbf{Q}, \omega)$ for $\alpha_S(T_c) = 0.90$ and 0.97 in Figs. 9(a)–9(d). When the system is away from the magnetic QCP [$\alpha_S(T_c) = 0.90$], the height of the hump structure in the s_{++} -wave state becomes small, as shown in Fig. 9(a). On the other hand, a sharp resonance structure still exists in the s_{\pm} -wave state, as shown in Fig. 9(b).

When the system is very close to the magnetic QCP [$\alpha_S(T_c) = 0.97$], a resonancelike peak structure is obtained in the s_{++} -wave state in Fig. 9(c). In the s_{\pm} -wave state, the resonance peak becomes very large, as shown in Fig. 9(d). We note that the peak structure in the s_{++} -wave state for $\alpha_S(T_c) = 0.97$ [Fig. 9(c)] is similar to that in the s_{\pm} -wave state for $\alpha_S(T_c) = 0.90$ [Fig. 9(b)]. These results suggest that results from neutron scattering experiments should be discussed carefully by considering the distance from the magnetic QCP.

IV. ANALYSIS: REASON FOR THE HUMP STRUCTURE IN THE s_{++} -WAVE STATE

Here, we discuss the origin of the resonance or hump structure in the dynamical spin susceptibility in the superconducting state. Below, we drop the orbital degrees of freedom for simplicity. The imaginary part of the spin susceptibility χ^S can be written in terms of the real and imaginary parts of bare susceptibility. We set $\Psi' = \text{Re}(\chi^0 + \phi^0)$ and $\Psi'' = \text{Im}(\chi^0 + \phi^0)$:

$$\chi^S = \frac{\Psi' + i\Psi''}{1 - U(\Psi' + i\Psi'')}. \quad (19)$$

Taking the imaginary part of χ^S , we obtain

$$\text{Im}\chi^S = \frac{\Psi''}{(1 - U\Psi')^2 + (U\Psi'')^2}. \quad (20)$$

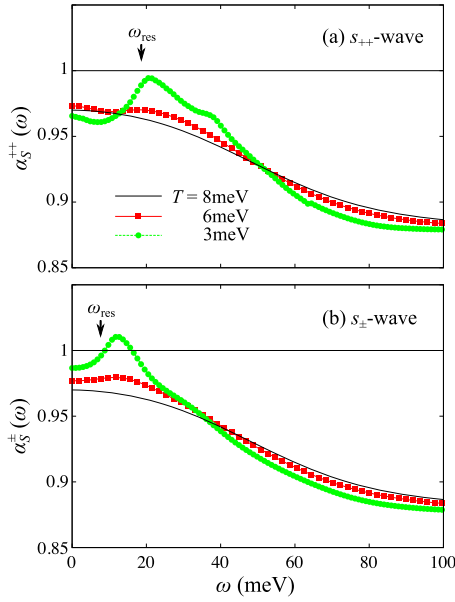


FIG. 10. Dynamical spin Stoner factor $\alpha_S(\omega)$ given by the FLEX for the (a) s_{++} and (b) s_{\pm} states. Here, U is fixed under the condition $\alpha_S(T_c) = 0.97$.

The denominator contains the term $U\Psi'$, which at $\omega = 0$ corresponds to the Stoner factor.

Here, we introduce the dynamical spin Stoner factor $\alpha_S(\omega)$, which is given by the largest real part of the eigenvalue of $\widehat{\Gamma}^S \widehat{\Psi}(\mathbf{q}, \omega)$ in the multiorbital model. $\alpha_S(\omega)$ at $\omega = 0$ is equivalent to α_S introduced in Sec. II D.

Figures 10(a) and 10(b) show, respectively, the dynamical spin Stoner factor for the s_{++} -wave state $\alpha_S^{++}(\omega)$ and that for the s_{\pm} -wave state $\alpha_S^{\pm}(\omega)$, given by the FLEX approximation. In both cases, we set $\alpha_S = 0.97$ at $T = T_c$. Both $\alpha_S^{++}(\omega)$ and $\alpha_S^{\pm}(\omega)$ take the maximum values at finite ω . In the s_{\pm} -wave state, at $T = 3$ meV, $\alpha_S^{\pm}(\omega)$ reaches unity at $\omega \approx 12$ meV, which corresponds to the resonance energy in the s_{\pm} -wave state shown in Fig. 8(b). In the s_{++} -wave state, at $T = 3$ meV, $\alpha_S^{++}(\omega)$ nearly reaches unity at $\omega \approx 20$ meV, which corresponds to the peak energy ω in the s_{++} -wave state in Fig. 8(a). Thus, the resonancelike peak structure in the s_{++} -wave state originates from the condition $\alpha_S^{++}(\omega) \approx 1$ at $\omega \approx \omega_{\text{res}}$.

To understand the role of the coherence factor, we also show the normal-part spin Stoner factors, $\alpha_{S,N}^{++}(\omega)$ and $\alpha_{S,N}^{\pm}(\omega)$, in Fig. 11. They are defined as the largest real part of the eigenvalue of $\widehat{\Gamma}^S \widehat{\chi}^0(\mathbf{q}, \omega)$ in the superconducting state. [The coherence factor due to $\widehat{\phi}^0(\mathbf{q})$ is dropped.] We set $\alpha_S = 0.97$ at $T = T_c$. Below T_c , both $\alpha_{S,N}^{++}(\omega)$ and $\alpha_{S,N}^{\pm}(\omega)$ increase with ω for $\omega \lesssim \omega_{\text{res}}$, reflecting the coherence peak in the density of states at $\omega = \pm\Delta^*$. $\alpha_{S,N}^{\pm}(\omega)$ is smaller than $\alpha_{S,N}^{++}(\omega)$ at $\omega \sim \omega_{\text{res}}$ since $\text{Im}\Sigma(\mathbf{k}, \omega)$ is larger in the s_{\pm} -wave state. By comparing Figs. 10 and 11, we find that the coherence factor enlarges (reduces) the dynamical spin Stoner factor in the s_{\pm} -wave (s_{++} -wave) state.

We note that the authors in Refs. [52,53] studied the Kondo insulator model using the dynamical mean-field theory and obtained a large hump structure in $\chi^S(\mathbf{q}, \omega)$ below the Kondo temperature. The origin of the hump structure of

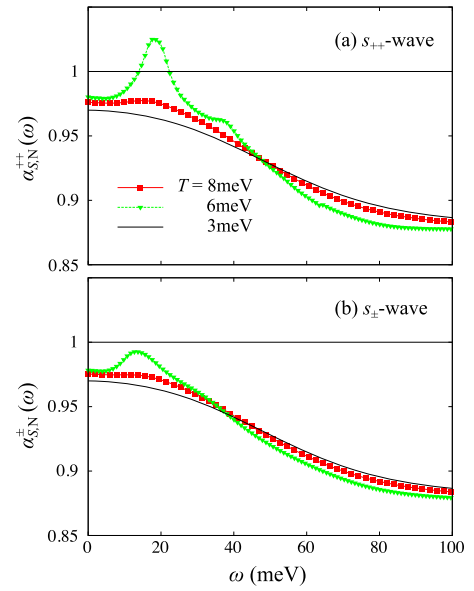


FIG. 11. Normal-part dynamical Stoner factor given by dropping $\widehat{\phi}^0(\mathbf{q})$ in Eq. (9) for the (a) s_{++} and (b) s_{\pm} states. Here, U is fixed under the condition $\alpha_S(T_c) = 0.97$.

χ^S in the Kondo insulator, which is actually observed in CeNiSn [54,55], is expected to be the same as that in the s_{++} -wave state, that is, the suppression of the inelastic scattering at low energies.

To summarize, we verified that $\alpha_S^{\pm}(\omega) \approx 1$ is realized in the s_{\pm} -wave state at the resonance energy $\omega = \omega_{\text{res}}$. The condition $\alpha_S^{++}(\omega) \lesssim 1$ at $\omega = \omega_{\text{res}}$ is also realized in the s_{++} -wave state. For $|\omega| \gtrsim 3\Delta^*$, $\alpha_S^{\pm}(\omega)$ and $\alpha_S^{++}(\omega)$ are suppressed by the large inelastic scattering $\gamma(\mathbf{k}, \omega)$ [39,40]. For this reason, $\text{Im}\chi^S(\mathbf{Q}, \omega)$ shows resonancelike behavior even in the s_{++} -wave state when the normal state is close to the magnetic QCP. We verified that, in the RPA without self-energy, $\alpha_S^{++}(\omega)$ for $T < T_c$ is smaller than $\alpha_S(\omega)$ at $T = T_c$ for any ω . For this reason, the RPA fails to reproduce the hump structure in the s_{++} -wave state in Figs. 8–9.

V. SUMMARY

In this paper, we studied the dynamical spin susceptibilities $\chi^S(\mathbf{q}, \omega)$ in the s_{++} -wave and s_{\pm} -wave states using the FLEX approximation. We calculated the low-temperature electronic states ($T \geq 1$ meV) accurately by using a very large number of Matsubara frequencies (2^{16}) based on the multistep FLEX method in Appendix A. In this method, we reduce the memory size of $\chi_{ll'mm'}^0(\mathbf{q}, i\omega_l)$ and $\phi_{ll'mm'}^0(\mathbf{q}, i\omega_l)$ by assigning crude \mathbf{k} meshes for high Matsubara frequencies ω_l . In the FLEX approximation in the superconducting state, α_S is approximately independent of T , as shown in Fig. 2. Near the magnetic QCP, α_S slightly increases below T_c in the s_{\pm} -wave state, whereas it decreases for $T \ll T_c$ in the s_{++} -wave state. This fact means that the expected phase diagrams for the s_{++} -wave and s_{\pm} -wave states do not have a pronounced difference, as schematically shown in Figs. 12(a) and 12(b). This result is consistent with the phase diagram given by the mean-field approximation in Ref. [56].

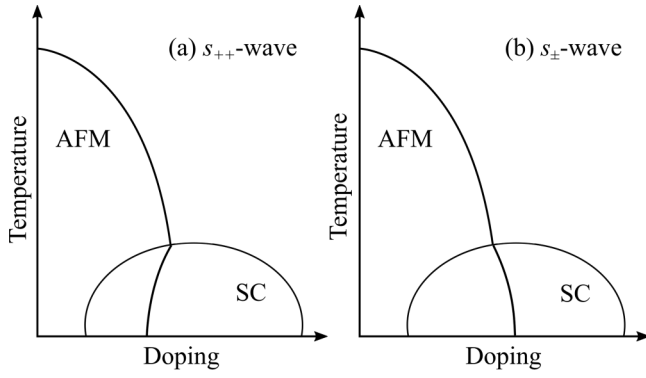


FIG. 12. Schematic magnetic-superconducting phase diagram expected from the Stoner factor in the superconducting state shown in Figs. 2 and 4: (a) s_{++} -wave state and (b) s_{\pm} -waves state.

We also studied the energy dependence of $\text{Im}\chi^S(\mathbf{q}, \omega)$ for $3 \text{ meV} \leq T \leq 8 \text{ meV} (= T_c)$ using the FLEX approximation. Figure 8 shows the numerical results in the case of $\alpha_S(T_c) = 0.95$, which would correspond to the optimally doped case. Then, we obtained sharp peak structures in $\text{Im}\chi^S(\mathbf{q}, \omega)$ at $\omega = \omega_{\text{res}}$ even in the s_{++} -wave state. The relation $\omega_{\text{res}} \sim 2\Delta^*$ holds in the s_{++} -wave state (see Fig. 4). In the s_{\pm} -wave state, the resonance peak is very sharp, and the resonance condition $\omega_{\text{res}} < 2\Delta^*$ is satisfied. Figures 9(a) and 9(b) show the results in the case of $\alpha_S(T_c) = 0.90$, which corresponds to the overdoped case. Then, the peak structures in $\text{Im}\chi^S(\mathbf{q}, \omega)$ in the s_{++} -wave state become tiny. In the s_{\pm} -wave state, the resonance peak is realized even in the overdoped case. These results confirm the self-energy driven resonancelike peak in the s_{++} -wave state, which was proposed in our previous semimicroscopic study [39,40]. That is, the enhancement in $\chi^S(\mathbf{q}, \omega)$ due to the self-energy effect (i.e., suppression of inelastic scattering below T_c) exceeds the suppression due to the coherence factor effect.

Both the ω and T dependences of the peak structure in the s_{++} -wave state near the magnetic QCP, shown in Fig. 8(a) [$\alpha_S(T_c) = 0.95$] and Fig. 9(c) [$\alpha_S(T_c) = 0.97$], resemble the experimental results in Na(Fe,Co)As and FeSe reported in Refs. [33,37]. Thus, characteristic inelastic neutron spectra in optimally doped Fe-based superconductors are well explained in the present FLEX study if the s_{++} -wave superconducting state is assumed. As the system approaches the magnetic QCP at $T = T_c$, which corresponds to the optimally doped case, $\text{Im}\chi^S(\mathbf{q}, \omega)$ smoothly changes to a resonancelike sharp peak structure ($\omega_{\text{res}} \approx 2\Delta^*$) in the s_{++} -wave state since α_S is very close to unity for $T \leq T_c$ in the FLEX approximation.

Since the overall (ω/Δ^*) dependence of $\text{Im}\chi^S(\mathbf{Q}, \omega)$ is insensitive to Δ^* for $T \lesssim 0.5T_c$, the present numerical results are reliable. We note that the resonancelike peak structure becomes sharper for smaller Δ^* at a fixed α_S .

In the FLEX approximation, both the coherence factor effect and self-energy effect on the dynamical susceptibility are taken into account on the same footing. In order to clarify the important role of the latter effect, we perform the RPA analysis in Appendix B. It is confirmed that the self-energy effect [(ω, T) dependence of the self-energy] discussed in

Refs. [39,40] is indispensable for the resonancelike peak in the s_{++} -wave state shown in Figs. 8(a) and 9(c).

ACKNOWLEDGMENTS

We are grateful to S. Onari for useful discussions. This work was supported by a Grant-in-Aid for Scientific Research from the Ministry of Education, Culture, Sports, Science, and Technology, Japan.

APPENDIX A: MULTISTEP METHOD OF THE FLEX APPROXIMATION

In the present study, we have to perform the FLEX approximation at low temperatures ($T \ll T_c$) accurately. For this purpose, however, very large numbers of Matsubara frequencies (from $-N_M$ to N_M) are required in the numerical study. To perform the FLEX at $T = 1 \text{ meV}$ precisely, for example, $N_M \sim 2^{16}$ is required. This fact has been preventing us from studying the FLEX approximation at very low temperatures. To solve this difficulty, we introduced the multistep FLEX method in the main text. In this method, we reduce the memory size of $\chi_{ll',mm'}^0(\mathbf{q}, i\omega_l)$ and $\phi_{ll',mm'}^0(\mathbf{q}, i\omega_l)$ by assigning fine \mathbf{q} meshes only for smaller $|\omega_l|$. We assign crude \mathbf{q} meshes for larger $|\omega_l|$ because the \mathbf{q} dependence of $\chi^0(\mathbf{q}, i\omega_l)$ is small then.

Here, we explain how to calculate the irreducible susceptibility $\chi^0(\mathbf{q}, i\omega_l)$ based on the multistep procedure. First, we introduce the set of number of momentum meshes and cutoff of Matsubara frequency number, $\{(N_q^{(i)}, N_M^{(1)}); i = 1, 2, \dots, L\}$. Here, $N_q^{(i)}$ ($N_M^{(i)}$) decreases (increases) with i . For example, we may set $(N_q^{(1)}, N_M^{(1)}) = (64^2, 16)$, $(N_q^{(2)}, N_M^{(2)}) = (32^2, 64)$, and $(N_q^{(3)}, N_M^{(3)}) = (16^2, 256)$ for $L = 3$. Then, we introduce the following irreducible susceptibility from the i th energy width:

$$\chi^{0(i)}(\mathbf{q}, i\omega_l) = -T \sum_n \sum_{\mathbf{k}}^{N_q^{(i)}} G^{(i)}(\mathbf{k} + \mathbf{q}, i\epsilon_n + \omega_l) G^{(i)}(\mathbf{k}, i\epsilon_n) \times [\Theta_i(\epsilon_n, \omega_l) - \Theta_{i-1}(\epsilon_n, \omega_l)], \quad (\text{A1})$$

where $G^{(i)}$ is the Green's function with meshes $(N_q^{(i)}, N_M^{(i)})$, $\Theta_i(\epsilon_n, \omega_l) = \theta(\epsilon_{N_M^{(i)}} - |\epsilon_n| + \delta) \theta(\epsilon_{N_M^{(i)}} - |\epsilon_n + \omega_l| + \delta)$, and $\Theta_0 = 0$. Then, the irreducible susceptibility in the multistep RPA or FLEX is given as

$$\chi^0 = \sum_{i=1}^L \chi^{0(i)}. \quad (\text{A2})$$

Note that $\chi^{0(i)}(\mathbf{q}, i\omega_l) = 0$ for $|\omega_l| > \omega_{N_M^{(i)}}$. (Since the \mathbf{q} -mesh number of $\chi^{0(i)}$ decreases with i , interpolation should be performed for larger i .) The obtained χ^0 is very similar to that given by the conventional RPA or FLEX using $(N_q^{(1)}, N_M^{(L)})$ since the \mathbf{q} dependence of $\chi^{0(i)}(\mathbf{q}, i\omega_l)$ is small when i or $|\omega_l|$ is large. In the same way, we introduce the self-energy from the i th energy width $\Sigma^{(i)}(\mathbf{k}, i\epsilon_n)$, and then the total self-energy is given as $\Sigma(\mathbf{k}, i\epsilon_n) = \sum_{i=1}^L \Sigma^{(i)}(\mathbf{k}, i\epsilon_n)$.

By employing this multistep FLEX procedure, calculation time and memory can be saved. In the present numerical research, we put $(N_q^{(1)}, N_M^{(1)}) = (128^2, 16)$, $(N_q^{(L)}, N_M^{(L)}) =$

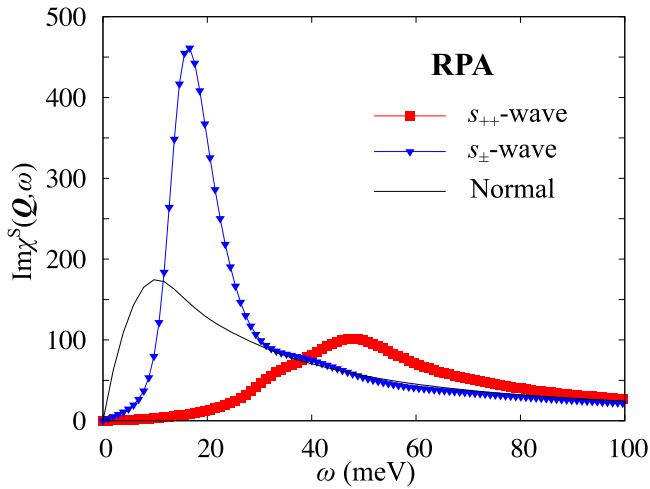


FIG. 13. Energy dependence of $\text{Im}\chi^S$ given by the RPA in the s_{++} -wave and s_{\pm} -wave states. $\text{Im}\chi^S$ in the normal state is also shown.

(2, 2^{16}), and $L = 6$. This multistep procedure is justified by the basic idea of coarse graining or renormalization in that the momentum dependence of physical quantities is moderate for higher energies.

APPENDIX B: DYNAMICAL SPIN SUSCEPTIBILITY GIVEN BY RPA

In this paper, we studied the dynamical spin susceptibility χ^S in both the s_{++} -wave and s_{\pm} -wave states by taking both the coherence factor effect and self-energy effect into account. Both effects are comparably important in strongly correlated superconductors [39,40]. For this purpose, we used the FLEX approximation, in which both the self-energy and χ^S are calculated self-consistently. Near the magnetic QCP, a resonancelike peak appears in the s_{++} -wave state since the enhancement in $\chi^S(\mathbf{q}, \omega)$ due to the self-energy effect (i.e., suppression of inelastic scattering below T_c) exceeds the suppression due to the coherence factor effect.

Here, we perform the RPA analysis in order to explain that the resonancelike peak in the s_{++} -wave state in Sec. III cannot be obtained once the self-energy effect is dropped. Figure 13 shows the energy dependence of $\text{Im}\chi^S$ in both the superconducting states ($T = 3$ meV) and normal states ($T = 8$ meV) given by the RPA. We set $U = 1.27$ eV for both normal and superconducting states, $\Delta_0 = 20$ meV in the superconducting states. The Stoner factor at $T = T_c$ is 0.98. In the RPA, the physical gap energy Δ_0^* discussed in the main text is equal to Δ_0 since the self-energy is absent. In the s_{\pm} -wave state, a clear resonance peak appears in $\text{Im}\chi^S$ at $\omega \approx \frac{1}{2}(2\Delta_0)$, consistent with previous RPA studies [27–32]. In contrast, in the s_{++} -wave state, the obtained $\text{Im}\chi^S$ is smaller than that in the normal state for $\omega < 2\Delta_0$. In addition, the hump structure at

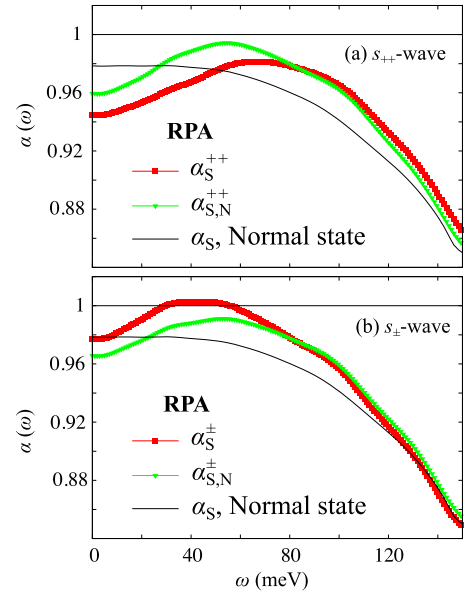


FIG. 14. Dynamical spin Stoner factor $\alpha_S(\omega)$ and the normal-part one $\alpha_{S,N}(\omega)$ given by the RPA for the (a) s_{++} -wave and (b) s_{\pm} -wave states. In $\alpha_{S,N}(\omega)$, the contribution from $\hat{\phi}^0(q)$ in Eq. (9) is dropped.

$\omega \gtrsim (2\Delta_0)$ is tiny. Therefore, the resonancelike peak structure in the s_{++} -wave state obtained by the FLEX approximation, discussed in the main text, cannot be obtained in the RPA. Thus, the self-energy effect [39,40] is indispensable for the resonancelike peak in the s_{++} -wave state.

In order to clarify the importance of the coherence factor, we show both the dynamical spin Stoner factor $\alpha_S(\omega)$ and the normal-part one $\alpha_{S,N}(\omega)$ given by the RPA in Figs. 14(a) and 14(b) for the s_{++} -wave and s_{\pm} -wave states, respectively. The difference between $\alpha_S(\omega)$ and $\alpha_{S,N}(\omega)$ originates from the coherence factor given by $\hat{\phi}^0(q)$ in Eq. (9). We see that $\alpha_{S,N}(\omega)$ is larger than $\alpha_S(\omega)$ in the normal state at $\omega \sim 2\Delta_0$ meV by reflecting the coherence peak in the density of states at $\omega = \pm\Delta_0$. [In Fig. 14, a small difference between $\alpha_{S,N}^+(\omega)$ and $\alpha_{S,N}^-(\omega)$ originates from the difference of $|\Delta(\mathbf{k})|$ in the s_{++} -wave and s_{\pm} -wave states in Eq. (5).] By including the coherence factor, $\alpha_{S,N}^+(\omega)$ [$\alpha_{S,N}^-(\omega)$] becomes smaller (larger) than $\alpha_S(\omega)$ in the normal state.

As we see in Fig. 14(a), the top of $\alpha_{S,N}^+(\omega)$ is comparable to that in the normal state. Therefore, we cannot expect the emergence of the resonancelike peak structure in the s_{++} -wave state in the RPA. In the FLEX approximation, $\alpha_{S,N}(\omega)$ below T_c becomes much larger than that in the normal state, as we show in Fig. 11. The reason is that the large $\gamma(\mathbf{k}, \omega)$ in the normal state, which suppresses the spin susceptibility, is reduced for $\omega \lesssim 3\Delta^*$ in the superconducting state. This self-energy effect [39,40] is indispensable for reproducing the resonancelike peak in $\text{Im}\chi^S$ in the s_{++} -wave state.

[1] K. Kuroki, S. Onari, R. Arita, H. Usui, Y. Tanaka, H. Kontani, and H. Aoki, *Phys. Rev. Lett.* **101**, 087004 (2008); K. Kuroki, H. Usui, S. Onari, R. Arita, and H. Aoki, *Phys. Rev. B* **79**, 224511 (2009).

[2] I. I. Mazin, D. J. Singh, M. D. Johannes, and M. H. Du, *Phys. Rev. Lett.* **101**, 057003 (2008).

[3] H. Kontani and S. Onari, *Phys. Rev. Lett.* **104**, 157001 (2010).

- [4] S. Onari, Y. Yamakawa, and H. Kontani, *Phys. Rev. Lett.* **112**, 187001 (2014).
- [5] Y. Yamakawa and H. Kontani, *Phys. Rev. B* **96**, 045130 (2017).
- [6] M. Yoshizawa, D. Kimura, T. Chiba, S. Simayi, Y. Nakanishi, K. Kihou, C-H. Lee, A. Iyo, H. Eisaki, M. Nakajima, and S. Uchida, *J. Phys. Soc. Jpn.* **81**, 024604 (2012).
- [7] Y. Gallais, R. M. Fernandes, I. Paul, L. Chauviere, Y.-X. Yang, M.-A. Measson, M. Cazayous, A. Sacuto, D. Colson, and A. Forget, *Phys. Rev. Lett.* **111**, 267001 (2013).
- [8] S. Onari, Y. Yamakawa, and H. Kontani, *Phys. Rev. Lett.* **116**, 227001 (2016).
- [9] Y. Yamakawa, S. Onari, and H. Kontani, *Phys. Rev. X* **6**, 021032 (2016).
- [10] S. Onari and H. Kontani, *Phys. Rev. Lett.* **109**, 137001 (2012).
- [11] H. Kontani and Y. Yamakawa, *Phys. Rev. Lett.* **113**, 047001 (2014).
- [12] R.-Q. Xing, L. Classen, and A. V. Chubukov, *Phys. Rev. B* **98**, 041108 (2018).
- [13] T. Yamashita, T. Takenaka, Y. Tokiwa, J. A. Wilcox, Y. Mizukami, D. Terazawa, Y. Kasahara, S. Kittaka, T. Sakakibara, M. Konczykowski, S. Seiro, H. S. Jeevan, C. Geibel, C. Putzke, T. Onishi, H. Ikeda, A. Carrington, T. Shibauchi, and Y. Matsuda, *Sci. Adv.* **3**, e1601667 (2017).
- [14] J. Li, Y. F. Guo, S. B. Zhang, J. Yuan, Y. Tsujimoto, X. Wang, C. I. Sathish, Y. Sun, S. Yu, W. Yi, K. Yamaura, E. Takayama-Muromachiu, Y. Shirako, M. Akaogi, and H. Kontani, *Phys. Rev. B* **85**, 214509 (2012).
- [15] S. Onari and H. Kontani, *Phys. Rev. Lett.* **103**, 177001 (2009).
- [16] Y. Yamakawa, S. Onari, and H. Kontani, *Phys. Rev. B* **87**, 195121 (2013).
- [17] D. V. Efremov, M. M. Korshunov, O. V. Dolgov, A. A. Golubov, and P. J. Hirschfeld, *Phys. Rev. B* **84**, 180512(R) (2011).
- [18] M. M. Korshunov, Y. N. Togushova, and O. V. Dolgov, *Phys. Usp.* **59**, 1211 (2016).
- [19] S. Iikubo, M. Ito, A. Kobayashi, M. Sato, and K. Kakurai, *J. Phys. Soc. Jpn.* **74**, 275 (2005).
- [20] M. Ito, H. Harashina, Y. Yasui, M. Kanada, S. Iikubo, M. Sato, A. Kobayashi, and K. Kakurai, *J. Phys. Soc. Jpn.* **71**, 265 (2002).
- [21] H. F. Fong, P. Bourges, Y. Sidis, L. P. Regnault, A. Ivanov, G. D. Gu, N. Koshizuka, and B. Keimer, *Nature (London)* **398**, 588 (1999).
- [22] C. Stock, C. Broholm, J. Hudis, H. J. Kang, and C. Petrovic, *Phys. Rev. Lett.* **100**, 087001 (2008).
- [23] P. Monthoux and D. J. Scalapino, *Phys. Rev. Lett.* **72**, 1874 (1994).
- [24] D. K. Morr and D. Pines, *Phys. Rev. Lett.* **81**, 1086 (1998).
- [25] A. Abanov and A. V. Chubukov, *Phys. Rev. Lett.* **83**, 1652 (1999).
- [26] T. Takimoto and T. Moriya, *J. Phys. Soc. Jpn.* **67**, 3570 (1998).
- [27] T. A. Maier and D. J. Scalapino, *Phys. Rev. B* **78**, 020514(R) (2008); T. A. Maier, S. Graser, D. J. Scalapino, and P. J. Hirschfeld, *ibid.* **79**, 224510 (2009).
- [28] M. M. Korshunov and I. Eremin, *Phys. Rev. B* **78**, 140509(R) (2008).
- [29] T. Das and A. V. Balatsky, *Phys. Rev. Lett.* **106**, 157004 (2011).
- [30] Y. Nagai and K. Kuroki, *Phys. Rev. B* **85**, 134521 (2012).
- [31] M. M. Korshunov, V. A. Shestakov, and Y. N. Togushova, *Phys. Rev. B* **94**, 094517 (2016).
- [32] M. M. Korshunov, *Phys. Rev. B* **98**, 104510 (2018).
- [33] Q. Wang, Y. Shen, B. Pan, Y. Hao, M. Ma, F. Zhou, P. Steffens, K. Schmalzl, T. R. Forrest, M. Abdel-Hafiez, X. Chen, D. A. Chareev, A. N. Vasiliev, P. Bourges, Y. Sidis, H. Cao, and J. Zhao, *Nat. Mater.* **15**, 159 (2016).
- [34] D. S. Inosov, J. T. Park, P. Bourges, D. L. Sun, Y. Sidis, A. Schneidewind, K. Hradil, D. Haug, C. T. Lin, B. Keimer, and V. Hinkov, *Nat. Phys.* **6**, 178 (2010).
- [35] S. Tatematsu, Y. Yasui, T. Moyoshi, K. Motoya, K. Kakurai, and M. Sato, *J. Phys. Soc. Jpn.* **80**, 073703 (2011).
- [36] M. Sato, T. Kawamata, Y. Kobayashi, Y. Yasui, T. Iida, K. Suzuki, M. Itoh, T. Moyoshi, K. Motoya, R. Kajimoto, M. Nakamura, Y. Inamura, and M. Arai, *J. Phys. Soc. Jpn.* **80**, 093709 (2011).
- [37] C. Zhang, H.-F. Li, Y. Song, Y. Su, G. Tan, T. Netherton, C. Redding, S. V. Carr, O. Sobolev, A. Schneidewind, E. Faulhaber, L. W. Harriger, S. Li, X. Lu, D. X. Yao, T. Das, A. V. Balatsky, T. Brückel, J. W. Lynn, and P. Dai, *Phys. Rev. B* **88**, 064504 (2013).
- [38] C. H. Lee, K. Kihou, J. T. Park, K. Horigane, K. Fujita, F. Waßer, N. Qureshi, Y. Sidis, J. Akimitsu, and M. Braden, *Sci. Rep.* **6**, 23424 (2016).
- [39] S. Onari, H. Kontani, and M. Sato, *Phys. Rev. B* **81**, 060504(R) (2010).
- [40] S. Onari and H. Kontani, *Phys. Rev. B* **84**, 144518 (2011).
- [41] N. E. Bickers, D. J. Scalapino, and S. R. White, *Phys. Rev. Lett.* **62**, 961 (1989).
- [42] C.-H. Pao and N. E. Bickers, *Phys. Rev. Lett.* **72**, 1870 (1994).
- [43] T. Dahm and L. Tewordt, *Phys. Rev. B* **52**, 1297 (1995).
- [44] M. Langer, J. Schmalian, S. Grabowski, and K. H. Bennemann, *Phys. Rev. Lett.* **75**, 4508 (1995).
- [45] S. Grabowski, M. Langer, J. Schmalian, and K. H. Bennemann, *Europhys. Lett.* **34**, 219 (1996).
- [46] J. J. Deisz, D. W. Hess, and J. W. Serene, *Phys. Rev. Lett.* **76**, 1312 (1996).
- [47] R. Putz, R. Preuss, A. Muramatsu, and W. Hanke, *Phys. Rev. B* **53**, 5133 (1996).
- [48] G. Esirgen and N. E. Bickers, *Phys. Rev. B* **55**, 2122 (1997).
- [49] S. Koikegami, S. Fujimoto, and K. Yamada, *J. Phys. Soc. Jpn.* **66**, 1438 (1997).
- [50] T. Kita, *J. Phys. Soc. Jpn.* **80**, 124704 (2011).
- [51] T. A. Maier, S. Graser, D. J. Scalapino, and P. Hirschfeld, *Phys. Rev. B* **79**, 134520 (2009).
- [52] T. Mutou and D. S. Hirashima, *J. Phys. Soc. Jpn.* **64**, 4799 (1995).
- [53] T. Mutou and D. S. Hirashima, *J. Phys. Soc. Jpn.* **63**, 4475 (1994).
- [54] H. Kadowaki, T. Sato, H. Yoshizawa, T. Ekino, T. Takabatake, H. Fujii, L. P. Regnault, and Y. Isikawa, *J. Phys. Soc. Jpn.* **63**, 2074 (1994).
- [55] S. Raymond, L. P. Regnault, T. Sato, H. Kadowaki, N. Pyka, G. Nakamoto, T. Takabatake, H. Fujii, Y. Isikawa, G. Lapertot, and J. Flouquet, *J. Phys.: Condens. Matter* **9**, 1599 (1997).
- [56] Y. Matsui, T. Morinari, and T. Tohyama, *J. Phys. Soc. Jpn.* **83**, 094703 (2014).